VIII. RADIO ASTRONOMY*

Academic and Research Staff

Prof. A. H. Barrett
Prof. B. F. Burke
Prof. R. M. Price
Prof. D. H. Staelin
J. W. Barrett
D. C. Papa
C. A. Zapata

Graduate Students

M. S. Ewing
H. F. Hinteregger
P. L. Kebabian
C. A. Knight
P. C. Myers
G. D. Papadopoulos
P. W. Rosenkranz
P. R. Schwartz
J. W. Waters
A. R. Whitney
T. T. Wilheit, Jr.
W. J. Wilson

RESEARCH OBJECTIVES AND SUMMARY OF RESEARCH

1. Very-long-baseline interferometric techniques have been used to study OH emission associated with H II regions and infrared stars. In particular, the intense OH emitter associated with the infrared star NML Cygni has been shown to comprise many small emitters with typical angular sizes of 0.08 second of arc and located within 2 seconds of arc of one another.

2. Observations of OH emission with a single antenna have continued with the use of the 140-ft radio telescope of the National Radio Astronomy Observatory, Green Bank, West Virginia. Approximately 500 infrared stars have been investigated for OH emission, and 24 have given positive results. Further studies of $O^{18}H$ have failed to show emission at a level of 1/3000 of the $O^{16}H$ emission. $O^{18}H$ has been detected in the absorption spectra of the galactic center at both 1637 MHz and 1639 MHz.

3. Observations of celestial H_2O have been made at Lincoln Laboratory, M. I. T., and at the National Radio Astronomy Observatory by observing the spectral line at 1.35 cm. A survey of 134 infrared stars has revealed 5 sources of H_2O emission. These include one Mira variable and one irregular variable. Further studies will attempt to correlate any changes in H_2O emission with changes in intensity at other wavelengths.

4. Microwave emission and absorption by atmospheric water vapor in the stratosphere has been extensively studied using the Haystack antenna of Lincoln Laboratory, M. I. T. This work has also included a redesign of a balloon payload to measure emission from molecular oxygen to test the inversion methods of determining the vertical temperature profile from the microwave emission.

5. Long-baseline interferometry for testing general relativity, and for geodetic measurements. A series of experiments has been conducted to measure the deflection of radio signals from quasars by the gravitational field of the sun. This is one of the classical tests of general relativity, and the aim is to refine the measurements to an accuracy of a few per cent, in order to set meaningful upper limits on the scalar character of the field. The measurements have also demonstrated the ability to synchronize clocks at remote locations with nanosecond accuracy, and the method is also

*This work was supported principally by the National Aeronautics and Space Administration (Grant NGL 22-009-016) and the National Science Foundation (Grant GP-14854); and in part by the Joint Services Electronics Programs (U. S. Army, U. S. Navy, and U. S. Air Force) under Contract DA 28-043-AMC-02536(E), the National Science Foundation (Grant GP-13056), and the Sloan Fund for Basic Research (M. I. T. Grant 312).

being applied to geodetic problems, with the eventual aim of measuring intercontinental distances to accuracies of a few centimeters. The rotation of the Earth can also be studied with a one order-of-magnitude improvement over current methods.

6. Long-baseline interferometry studies of H_2O emission. A series of experiments is under way to measure the angular sizes of the stronger H_2O sources. The 85-ft telescope of the Naval Research Laboratory, the 140-ft telescope of NRAO, and the 120-ft Haystack telescope of Lincoln Laboratory, M.I.T., are being used for this experiment.

7. Aperture synthesis at 1.7 cm wavelength. An interferometer has been constructed and is now working at 1.7 cm wavelength, with the use of a small computer (PDP-8) for real-time data processing and control. The system demonstrates the feasibility of aperture synthesis at this short wavelength, and measurements will continue.

8. Pulsar studies. A 200-ft diameter antenna has been constructed for studies of pulsars at frequencies in the range 100-300 MHz. The antenna is a phased array of 16 spherical reflectors, each 50 ft in diameter. The array can work to zenith angles of 45°, and can be used at several frequencies simultaneously.

9. Pulsar observation. A long-term observing program has been conducted at NRAO, Green Bank, West Virginia, using the 300-ft transit telescope. The discovery of the pulsar in the Crab Nebula was an early result during the past year, and observations continue. The pulse shape, frequency structure, and intensity variations in time of a number of pulsars are being studied, with the intention of identifying those features of the radiation intrinsic to the source, so that meaningful tests of pulsar theories can be made. Initial results of these programs include (i) detection of systematic motion of subpulses across pulses in three new pulsars, (ii) measurement of very strong frequency dependence of average pulse shapes in NP0532, (iii) studies of 0.1-ms structure in several pulsars, (iv) studies of the frequency dependence of scintillation phenomena, including detection of transient spectral features narrower than 10 kHz, and (v) anomalous sharp transitions in the behavior of MP0031.

A. H. Barrett, B. F. Burke

A. SEARCH FOR INTERSTELLAR $O^{18}H$ IN EMISSION

In August 1969, we made a search for interstellar $O^{18}H$ in emission from the strong $O^{16}H$ emission sources W3 and W49. The observations were made with the 140-ft (43-m) radio telescope of the National Radio Astronomy Observatory, located in Greenbank, West Virginia. The antenna was equipped with a scalar feed and two cooled parametric amplifiers. With this system it was possible to simultaneously measure two orthogonal linear polarizations. The two system noise temperatures were approximately 70°K. Spectral line processing was performed by using two 192 channel autocorrelators — one on each polarization. The output spectra obtained from each correlator were added to give the unpolarized S_o spectrum.

The spectra from the search are shown in Figs. VIII-1 and VIII-2. The upper part of each figure shows the $O^{18}H$ spectra (under the assumption of a rest frequency of 1637.46 MHz), and the corresponding main line emission spectrum (f_o = 1665.401) taken with the same frequency resolution on the same date is plotted in the lower part of the figure. A second-order curve has been subtracted from the uniformly weighted

$O^{18}H$ spectra; however, because of a large amount of curvature in the preamplifier bandpass during the W3 observations, a higher order curve is still evident.

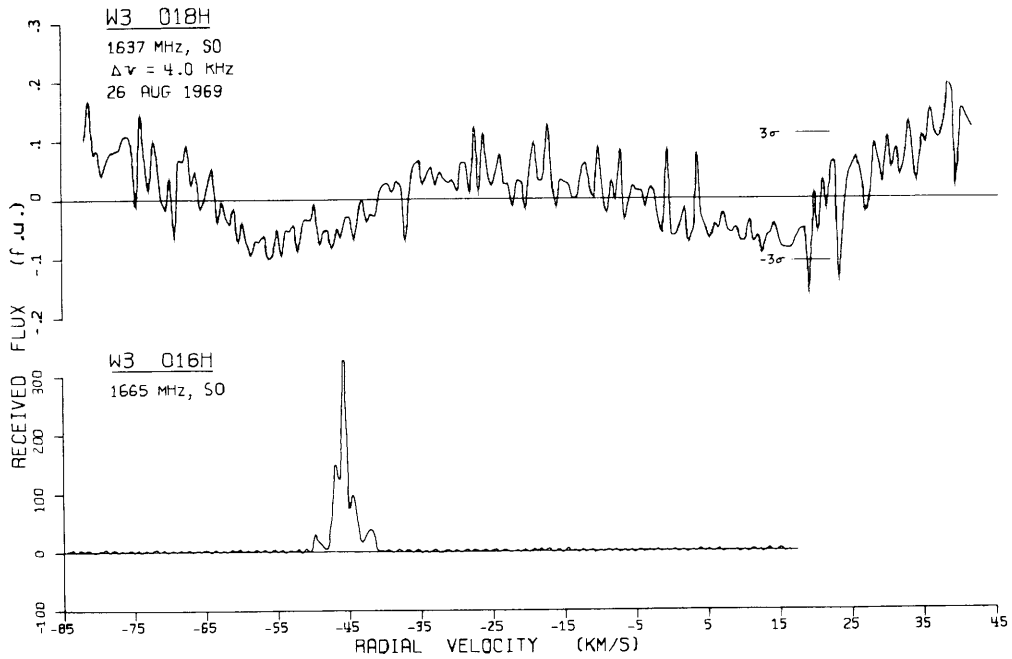

Fig. VIII-1. Spectra of the OH source W3 as observed in $O^{18}H$ (f_o = 1637.46 MHz) and in $O^{16}H$ (f_o = 1665.358 MHz). The spectra are plotted in flux units (1 f.u. = 10^{-26} w · m^{-2} · Hz^{-1}) and the flux scales are in the ratio 1:1000. The unpolarized S_o spectra were obtained by adding two orthogonal linearly polarized spectra. An overlap frequency-switching method was used for the $O^{18}H$ spectra which gave an effective integration time of 34.4 h in the central portion (-61 to +14 km sec^{-1}) and 17.2 h at either edge. The measured 3σ lines refer to the central portion of the $O^{18}H$ spectrum.

From these data it is possible to establish an upper limit for the $O^{18}H$ emission from W3 and W49 of 1/2000 to 1/3000. The previous limit for $O^{18}H$ emission was 1/800 (Wilson and Barrett[1]). Using the emission velocity of the 1665 MHz emission, the 1/3000 limit is applicable over the frequency range 1637.13-1637.53 MHz, while the 1/2000 limit applies over the complete search range 1637.02-1637.64 MHz. Barrett and Rogers have calculated the frequency of this line ($^2\pi_{3/2}$, J = 3/2, F = 1 → 1) as 1637.30 ± 0.2 MHz. We have measured the frequency of this line in absorption against Sgr A as 1637.5 ± 0.1 MHz (Wilson and Barrett[1]).

Ball and Penfield[3] have pointed out, that $O^{18}H$ maser emission could be detected if (i) the abundance ratio of O^{18}/O^{16} were near the terrestrial abundance ratio of 1/490,

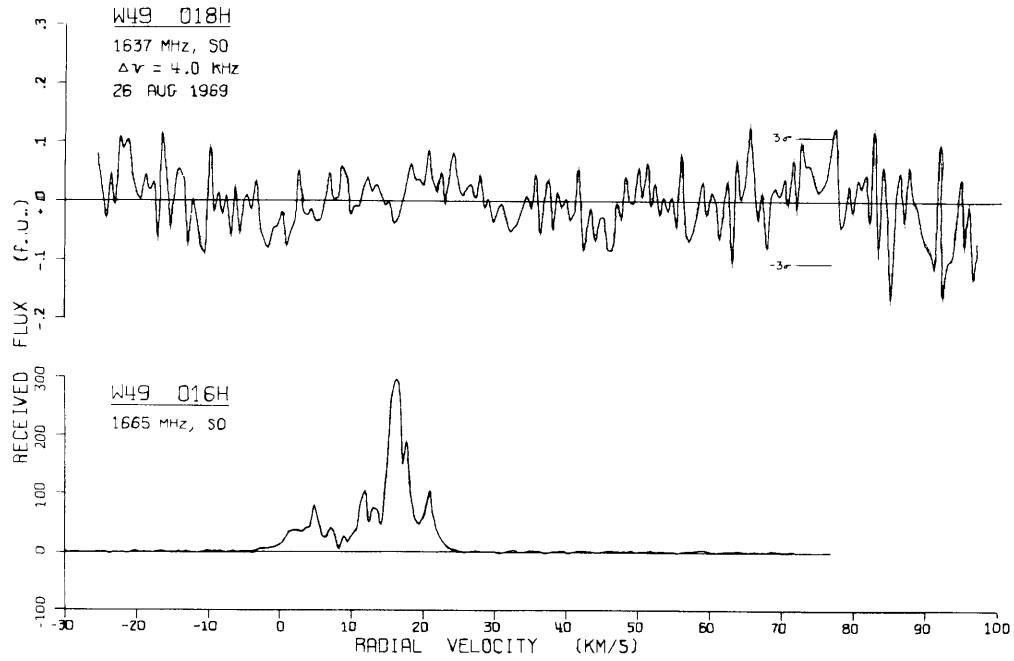

Fig. VIII-2. Spectra of the OH source W49 as observed in $O^{18}H$ (f_o=1637.46 MHz) and in $O^{16}H$ (f_o = 1665.358 MHz). The unpolarized S_o spectra were obtained by adding two orthogonal linearly polarized spectra. An overlay frequency-switching technique was used for the $O^{18}H$ spectra which gave an effective integration time of 38 h in the central portion (-6 to +71 km sec^{-1}) and 19 h at either edge. The measured 3σ lines refer to the central portion of the $O^{18}H$ spectrum.

(ii) the maser pumping mechanism is independent of isotropic species, and (iii) the $O^{18}H$ maser is fully saturated as is probably the $O^{16}H$ maser. Since we can expect that the abundances could have approximately the terrestrial value, and that the pumping of the OH to excited states (either by UV or IR) would be independent of the isotropic species, the negative result obtained here implies that the $O^{18}H$ maser is unsaturated and thus undetectable. Since the $O^{16}H$ emission is believed to be saturated at 1665 MHz in W3 and W49 (on account of the high degree of circular polarization and lack of time variations), this result places constraints on the degree of saturation of the $O^{16}H$ maser.

W. J. Wilson, A. H. Barrett

References

1. W. J. Wilson and A. H. Barrett, Quarterly Progress Report No. 90, Research Laboratory of Electronics, M. I. T., July 15, 1968, p. 9.
2. A. H. Barrett and A. E. E. Rogers, Nature 204, 62 (1964).
3. J. A. Ball and H. Penfield (to appear in the Astrophysical Journal).

B. WATER-VAPOR EMISSION ASSOCIATED WITH INFRARED STARS

During September and October 1969, we surveyed 134 red stars and stellar objects for anomalous water-vapor emission at 1.35 cm and detected 5 objects including VY Canis Majoris (Knowles et al.[1,2]), R Aquilae (Turner et al.[3]) and 3 new water-vapor sources. Observations were made with the 36.5 m "Haystack" antenna of Linclon Laboratory, M.I.T., with a receiver consisting of a degenerate parametric amplifier with a balanced-mixer second stage, a local oscillator synthesized from the third harmonic of a 7.4 GHz phase-locked oscillator and a 100-channel autocorrelator. The antenna's aperture efficiency, including radome losses, was ~15% at 45° elevation angle and the total radiometer system temperature, including atmospheric and radome contributions, was between 1300°K and 1600°K for spectral-line observations. For our survey, the system was operated at total power with equal times spent on source and 1° off source for comparison. Each star was observed at 4 overlapping windows, 4 MHz wide, with 100-kHz resolution giving a total coverage of ±100 km/sec relative to the local standard of rest. No search in position was made because the 1.3' beam is much larger than the

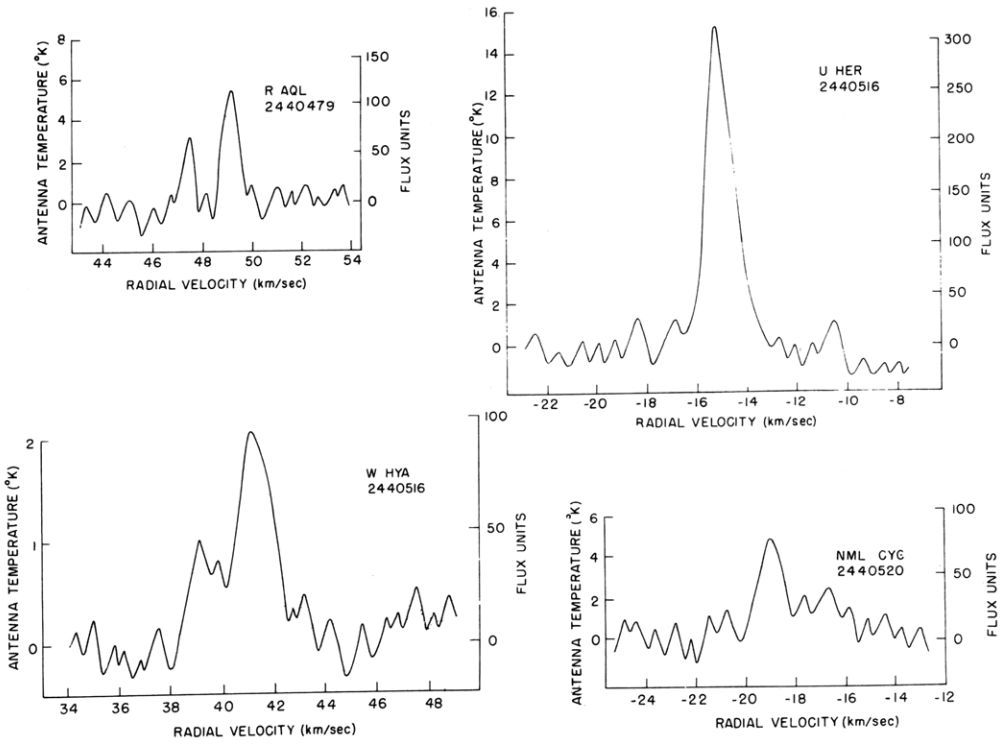

Fig. VIII-3. Water-vapor spectra of R Aql, U Her, W Hya and NML Cyg with 30-kHz (0.4 km/sec) resolution.

uncertainties of star positions and the antenna pointing errors are less than half a beamwidth. Antenna pointing and system performance were periodically checked by observation of the water-vapor sources W3, W3OH, W49, and Orion A. The detection limit of the survey was ~10 flux units.

In Fig. VIII-3, spectra of the water-vapor sources R Aql, U Her, W Hya and NML Cyg are shown with 30-kHz resolution (cosine weighting for the autocorrelation function was used). The fifth source, VY CaM, has been discussed elsewhere (Knowles et al.[1,2], Meeks et al.[4]) and was only included in our survey for completeness. In these spectra, we give both the observed antenna temperature for the sum of left and right circular polarization and the flux that has been corrected for atmospheric absorption and antenna gain-elevation dependence. The radial velocities are relative to the local standard of rest and are computed for a line rest frequency of 22,235,080 kHz.

In Table VIII-1 we have listed the optical, infrared and radio properties of the four observed sources as well as the Julian date of our first observation and the exact position on that date. It is interesting to note that, although the four stars have very similar spectral types and infrared color indices and three of them are long-period variables, there are some striking differences in their microwave and infrared spectral properties. R Aql and NML Cyg (as well as VY CaM) are bright Type IIb OH sources exhibiting both 1612-MHz and main-line emission and, thus, are somewhat similar to the majority of the other known water-vapor sources (Turner et al.[3]). W Hya and U Her, however, show no 1612-MHz emission (Wilson[9]). We searched for 1665-MHz OH emission from U Her on 23 October 1969 using "Haystack," and found no spectral line greater than 0.5 flux unit in the velocity interval -85 km/sec to +55 km/sec, so this source does not appear to be a Type I OH source either and, therefore, is similar to the W3 water-vapor source (Meeks et al.[4]). In the infrared, both W Hya and R Aql show strong water-vapor absorption bands, and, since U Her is also a Mira variable, it probably also shows water absorption (Spinrad and Vardya,[10] Moroz[11]); NML Cyg, however, does not show water-vapor bands but may show absorption from interstellar ice (Johnson[12]).

For the long-period variables W Hya, U Her, and R Aql the radial velocity of the microwave emission indicates that it originates in the atmospheres of these stars, probably at radii intermediate between the regions responsible for optical emission and absorption. The fact that water-vapor emission is detectable near maximum light for one star (U Her), and, with Turner's observations taken into account, near both maximum and minimum in R Aql is rather interesting. Infrared observations indicate a variation in water-vapor absorption with phase in some Mira variables with minimum absorption occurring near maximum light (Sinton[13]). Infrared water-vapor absorption has been interpreted thermally, and variations with phase are explained as a decrease in molecular concentration near maximum light because of photodissociation of the water molecule. Any conceivable water-vapor emission mechanism is critically dependent upon molecular

Table VIII-1. Microwave, optical, and infrared properties of the observed water-vapor sources.

Name (IRC)[7]	J.D.	R.A. (1969.7) DEC. (1969.7)	Sp. Type Class	Period (days)[5] Phase	OH:y/n, V_{LSR}[6]	H_2O:V_{LSR}	I-K[7]	Optical/IR Lines[8]
W Hydrae (-30207)	2440516	13H47M19.1S -28°13'0.6"	M8e SRa	382.2	1612:n	39,41		e:31 a:45
U Herculis (+20298)	2440516	16H24M26.3S 18°57'43.1"	gM7e-M8e M	406.0 0.05	1612:n 1665:n	-13	4.2	e:-26 a:-10
R Aquilae (+10406)	2440479	19H4M53.3S 8°10'39.9"	gM5e-M8e M	300.3 0.44	1612:y,43,54 1665:n 1667:y,43 1720:n	47,49	5.0	e:38 a:52
NML Cygni (+40448)	2440520	20H45M17.8S 40°0'39.9"	M6 IR Star		1612:y,-22,20 1665:y,-13,-20 1667:y,14,25 1720:n	-19	8.2	

5. Margaret W. Mayall, Private communication, AAVSO, 1969.
6. W. J. Wilson, A. H. Barrett, and J. M. Moran (to appear in Astrophys. J.).
7. G. Neugebauer and R. B. Leighton, NASA, Washington, D.C., 1969.
8. P. W. Merrill, Astrophys. J. 94, 171, 1941.

concentration, and a change of one or two orders of magnitude should be very strongly amplified by the emission mechanism and appear as violent time variations. At least for R Aql, we do not believe that such violent time variations are indicated by the microwave data. We suggest that, in the possible presence of the gross population anomalies necessary to produce microwave emission, a thermal interpretation of the water-vapor spectrum in these stars is open to question. Simultaneous study of the infrared and microwave water-vapor lines in Mira variables with changes in radial velocity and angular size, as well as intensity, should provide a unique opportunity to investigate the water-vapor emission mechanism.

Water-vapor emission from the IR star OH source NML Cyg has not been found in previous searches (Meeks et al.,[4] Turner et al.[3]), but was found in our search, probably because of our much higher sensitivity. Although time variations cannot be ruled out for any water-vapor source, we do not believe that positive proof of variability for NML Cyg exists. The discovery of water-vapor emission in NML Cyg gives further evidence that this source and VY CaM form a class of infrared-microwave objects distinct from the other IR star OH or H_2O sources which are typically Mira variables (Wilson, Barrett, and Moran[6]).

The authors are indebted to J. C. Carter who engineered the radiometer system and encouraged our observations, and to W. J. Wilson for his many discussions and the use of his data before publication. We also wish to thank our tireless observers T. E. Beeskau and C. A. Zapata, and Dr. M. L. Meeks and the staff of Lincoln Laboratory* for their support.

P. R. Schwartz, A. H. Barrett, P. W. Rosenkranz

References

1. S. H. Knowles, C. H. Mayer, A. C. Cheung, D. M. Rank, and C. H. Townes, Science 163, 1055 (1969).
2. S. H. Knowles, C. H. Mayer, W. T. Sullivan, and A. C. Cheung, Science 166, 221 (1969).
3. B. E. Turner, D. Buhl, E. B. Churchwell, P. G. Mezger, and L. E. Snyder (to appear in Astronomy and Astrophysics).
4. M. L. Meeks, J. C. Carter, A. H. Barrett, P. R. Schwartz, J. W. Waters, and W. E. Brown, Science 165, 180 (1969).
5. Margaret W. Mayall (Private communication, AAVSO, 1969).
6. W. J. Wilson, A. H. Barrett, and J. M. Moran (to appear in Astrophys. J.).
7. G. Neugebauer and R. B. Leighton, Two Micron Sky Survey – A Preliminary Catalog, N. A. S. A., Washington, D. C., 1969.
8. P. W. Merrill, Astrophys. J. 94, 171 (1941).

*Lincoln Laboratory is operated by the Massachusetts Institute of Technology with the support of the U. S. Air Force.

9. W. J. Wilson (Private communication, 1969).

10. H. Spinrad and M. S. Vardya, Astrophys. J. 146, 399 (1966).

11. V. I. Moroz, Soviet Astron. – AJ 10, 47 (1966).

12. H. L. Johnson, Astrophys. J. 154, L125 (1968).

13. W. M. Sinton, "Stellar Spectra," in Infrared Astronomy, P. J. Brancazio and A. G. W. Cameron (eds.) (Gordon and Breach, New York, 1968).

C. PULSAR RADIO-EMISSION MECHANISMS

It is often argued that radio emission from pulsars must be generated by a coherent emission process, because of the very high surface brightnesses which are observed. These observed brightnesses are generally based upon assumed source sizes of approximately 30 km, which follows from the assumption that the observed 10^{-4} s time structure can be generated only by a source of size 10^{-4} c = 30 km. An incoherent source of this size would require particles with energies well in excess of 10^{20} eV, which is too high to be plausible; hence, it is indicated that coherent processes are required.

If we assume the general pulsar geometry shown in Fig. VIII-4, then the source size could be substantially larger than 30 km, and yet be consistent with 10^{-4} s time variations. The model assumes simply that a narrow stream of particles is ejected from the rotating star. In the illustrated example, for pulsar CP1919, the required particle energies are of the order of 10^{12} eV, a value consistent with predicted particle

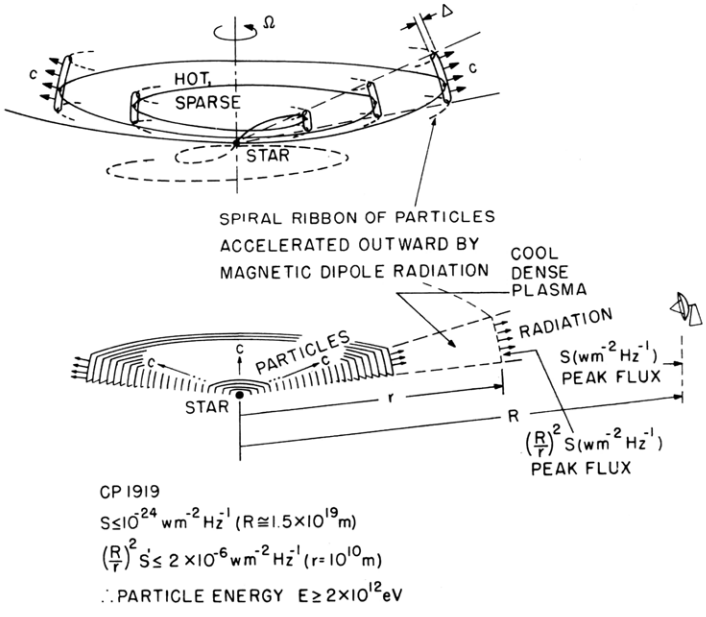

Fig. VIII-4. Pulsar geometry.

acceleration mechanisms. Still lower particle energies are plausible, since the radius r at which the outward-moving spiral of relativistic particles is converted to a spiral of photons is almost arbitrary. The thickness Δ of the spiral is dictated by the details of the near fields around the neutron star, and a thickness of 30 km appears reasonable, since the star itself is approximately that size.

The principal difficulty associated with this model appears to be the low cross sections for common processes by which 10^{12} eV particles can radiate much energy before travelling distances comparable to their Larmor radius. Such processes are being examined to see if any are consistent with the data.

D. H. Staelin

D. LOW TIME-RESOLUTION PULSAR OBSERVATIONS

We have continued multichannel, low time-resolution observations of pulsars at the National Radio Astronomy Observatory, Green Bank, West Virginia. During November 1969, a 50-channel spectrometer with 10-kHz resolution was used for the first

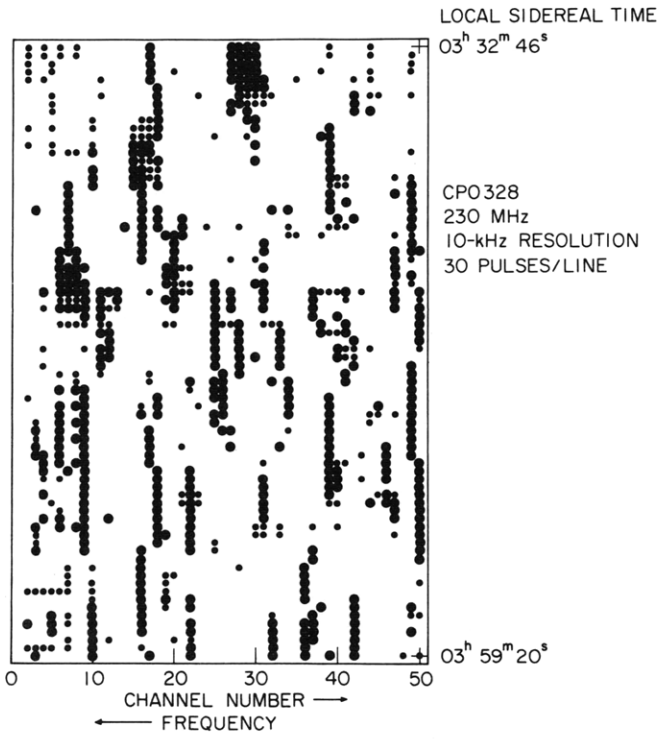

Fig. VIII-5. Threshold plot of CP0328 spectrum against time. The center frequency is 230 mHz, the bandwidth per channel is 10 kHz. Each horizontal line is an average of 30 consecutive pulse spectra. Fifty frequency channels are represented in increasing order from right to left. Two arbitrarily chosen threshold levels are represented as small and large dots. (Data taken November 10, 1969.)

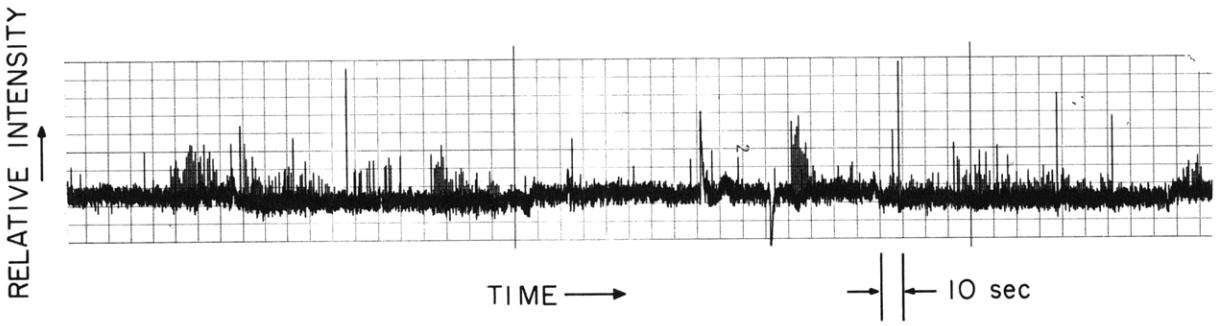

Fig. VIII-6. Analog recording of pulses of MP0031 taken with 500-kHz bandwidth at 168.5 mHz. One horizontal division represents 10 s of time. The recorder time constant was 0.02 s. (Data taken August 14, 1969.)

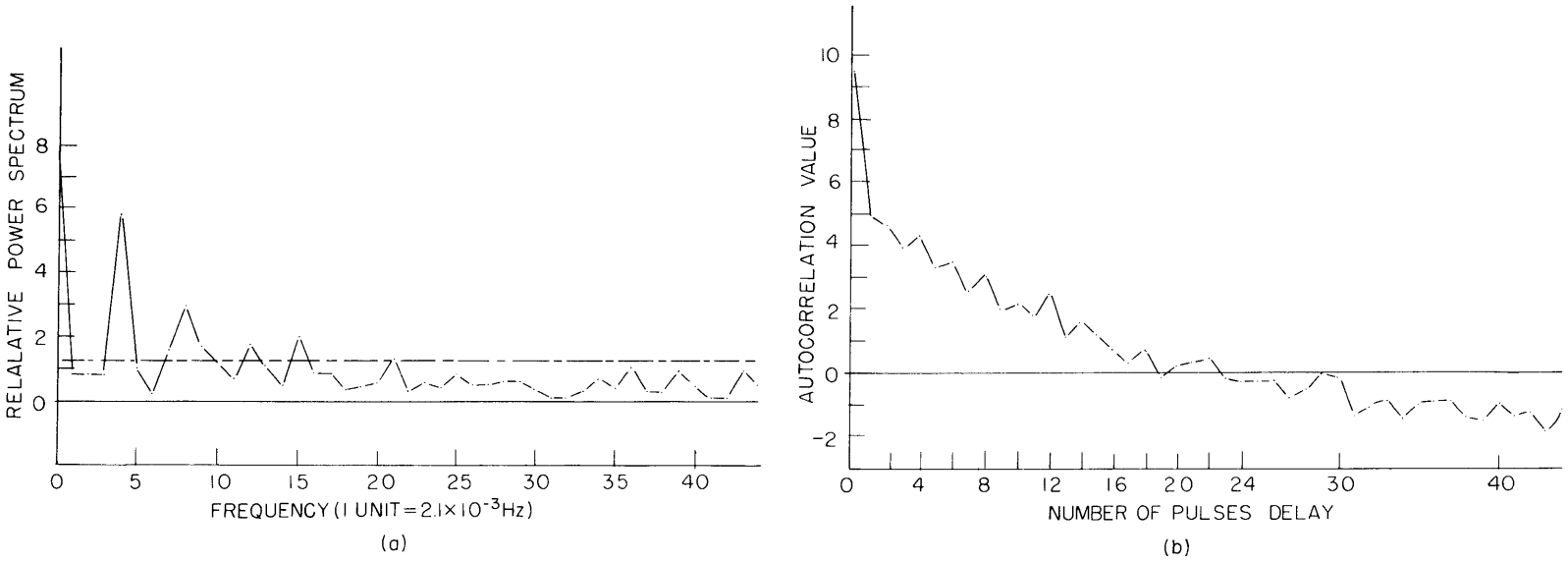

Fig. VIII-7. (a) Relative power spectrum of 512 consecutive pulse amplitudes of MP0031. The pulses were averaged from 163.5 mHz to 168.5 mHz. Dashed line represents the approximate peak noise level. Note significant peaks at 4, 8, 12, and 15 frequency units. (Data taken August 15, 1969.)
(b) Autocorrelation function of the same pulse amplitudes averaged from 165.2 MHz to 166.6 MHz. The mean value was subtracted from the data before correlation.

time on the 300-ft antenna.

Several new phenomena have been recognized in the frequency and time dependencies of pulsar signals. Very narrow-frequency structure has been found in the spectrum of pulses of CP0328 at frequencies near 200 MHz. Some features are unresolved at 10-kHz bandwidth. A plot of representative data is presented in Fig. VIII-5. Narrow features are seen to persist over times of a few minutes. We feel that further observations with higher frequency resolution and taken over longer times are required to characterize the statistical nature of the spectrum of this source.

Pulse-to-pulse amplitude variations in the pulsar MP0031 appear to be anomalous in comparison with those of other sources. A discretely varying modulation is apparently operating on the basic pulse period (see Fig. VIII-6). The sharply defined bursts are characteristically reflected in the power spectrum of the pulse amplitudes (Fig. VIII-7a). The corresponding correlation function is given in Fig. VIII-7b; the characteristic burst width in this case appears to be 10-15 pulses. The power spectrum and correlation function will vary somewhat over a 1/2-h scan.

M. S. Ewing, R. A. Batchelor, D. H. Staelin,
R. M. Price, B. F. Burke

E. PULSAR OBSERVATIONS WITH A SWEPT-FREQUENCY LOCAL OSCILLATOR

In September and November 1969, observations were made of pulsars with a swept-frequency local oscillator and a 50-channel spectrum analyzer. The September observations were made, as earlier runs, with the local oscillator swept linearly. By November, modifications had been made by the National Radio Astronomy Observatory staff to allow a second-order correction to be added to the sweep rate in order to precisely track the dispersed pulses.

Observations were carried out at 160 MHz and 115 MHz with 10-kHz filters on the 50-channel receiver. This gave an improvement of three over the previous time resolution achieved with the system. The effective time resolutions are 1.2 ms and 3.6 ms for 160 MHz and 115 MHz, respectively. These high time resolution observations confirmed the decay-time constants reported previously for pulses from the Crab Nebula pulsar, NP0532.[1]

Observations of CP0834 carried out in August 1969 have been further analyzed, and the bandwidth of some of the frequency features of the pulses examined. An effective frequency resolution of approximately 1 MHz can be achieved with the present system. This, in conjunction with the high time resolution, allows us to determine more completely the structure of the pulses.

Figure VIII-8 shows plots of pulse intensity as a function of frequency across a band

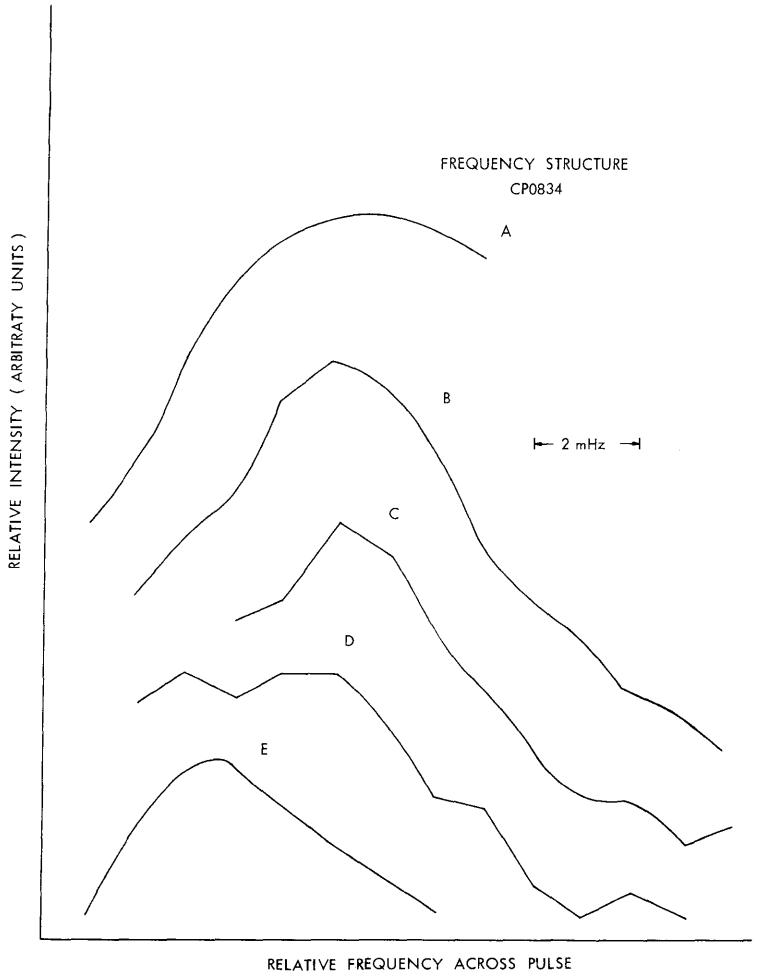

Fig. VIII-8. Frequency structure in CP0834. Plots show integrated pulse intensity as a function of frequency across a band centered at 153.5 MHz. Pulses build up or decay to half-intensity over frequency intervals of 2-8 MHz. Curve B shows a discrete frequency feature on a pulse, whereas other curves show growth or decay of pulses. Curve E shows a rapid build-up associated with the development of a double pulse (in the time domain) and subsequent change to a single pulse as it decays.

centered at 153.5 MHz. The examples given show pulses growing or falling off to half-intensity over an interval of several MHz (ranging from 2 MHz to 8 MHz, in general). More rapid increases or decreases are generally associated with complex time structure within the pulse, for example, going from a single to a double pulse.

R. M. Price, D. H. Staelin, J. Sutton

(Dr. J. Sutton is with the National Radio Astronomy Observatory.)

References

1. D. H. Staelin, J. Sutton, and M. S. Ewing, Quarterly Progress Report No. 95, Research Laboratory of Electronics, M.I.T., October 15, 1969, p. 3.

F. GALACTIC CONTINUUM STRUCTURE

As part of a continuing galactic structure program, observations were carried out with the 1000-ft dish of the Arecibo Ionospheric Observatory, in Puerto Rico, at a frequency of 318 MHz. At this frequency, the HPBW of the telescope is 16 minutes of arc. A much improved feed system allowed sources down to less than 0.1 flux unit to be detected (one flux unit = 10^{-26} W/M^{2}Hz).

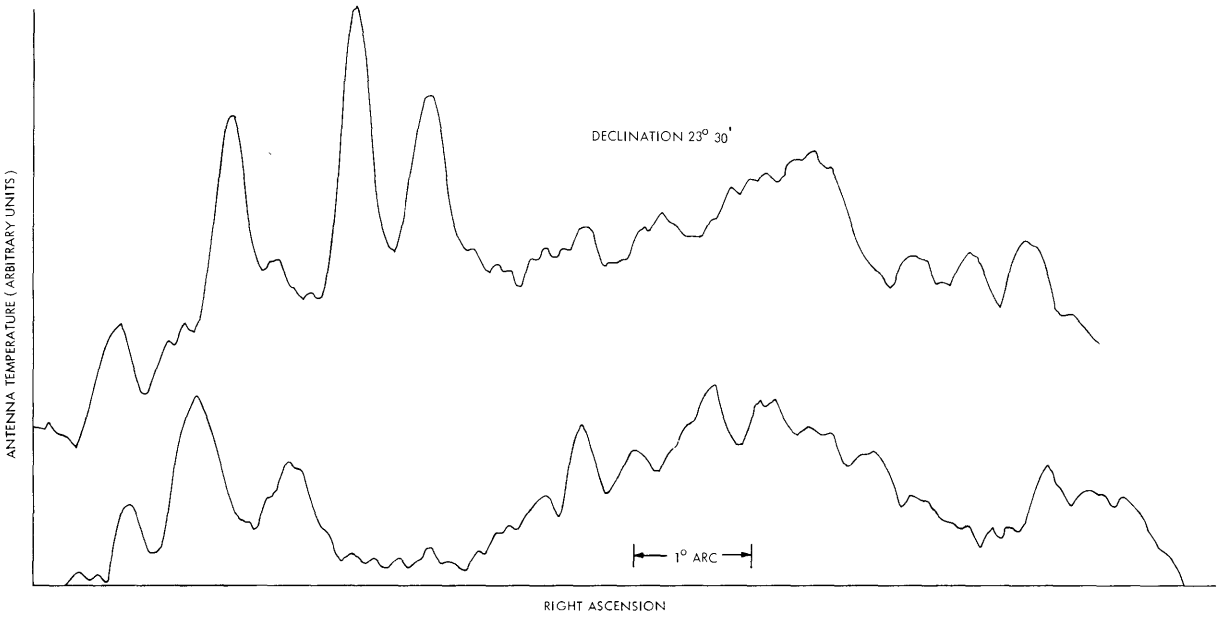

Fig. VIII-9. Scans with a 16 minutes of arc HPBW at 318 MHz in two different medium-latitude regions of the Galaxy. Structure up to several degrees in extent can be seen.

With this resolution the galactic disk still appears to be continuous and is not broken up into obvious emission regions. Out of the plane regions up to several degrees in extent were noted and are being studied in detail. Figure VIII-9 shows the structure typical of much of the medium latitude portions of the galaxy.

R. M. Price

G. VERY LONG BASELINE INTERFEROMETRY FOR H_2O SOURCES

The two K-band radiometers to be used in this experiment were locked to two independent rubidium standards and then tested for synchronism. The test arrangement

is shown in Fig. VIII-10. In Fig. VIII-11 the 100-kHz beat output is compared with a 100-kHz reference tone taken from one of the rubidium standards; the exposure time was 10 s.

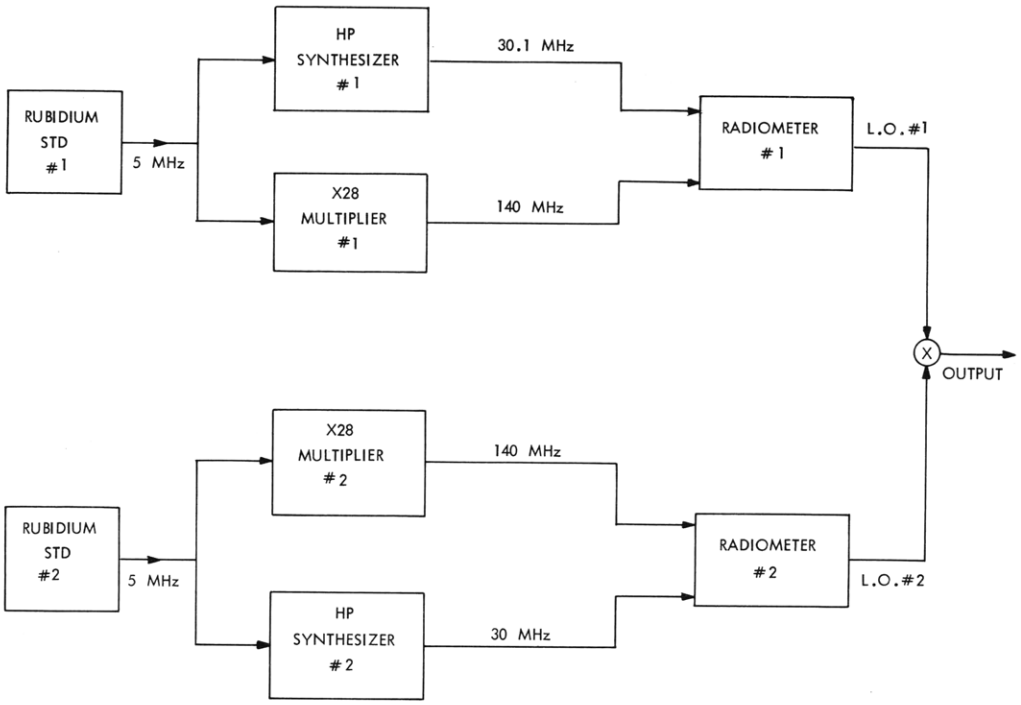

Fig. VIII-10. K-band phase stability arrangement.

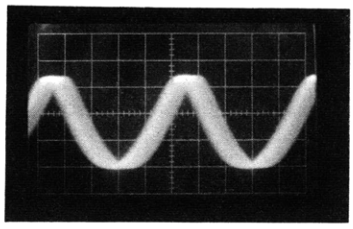

Fig. VIII-11. Phase comparison.

From the tests that were performed we have concluded that the rms phase noise is less than 15°, and that the two local oscillators stay in synchronism to within 60° for an interval of 10 s.

G. Papadopoulos, B. F. Burke, D. C. Papa,
J. W. Barrett, P. R. Schwartz

H. Ku-BAND INTERFEROMETER

1. System Phase Stability

The phase stability of the interferometer was determined by feeding the same cw signal (17.19 GHz) to the feed inputs of both radiometers and monitoring the output of the analog multiplier. The schematic of the arrangement is shown in Fig. VIII-12.

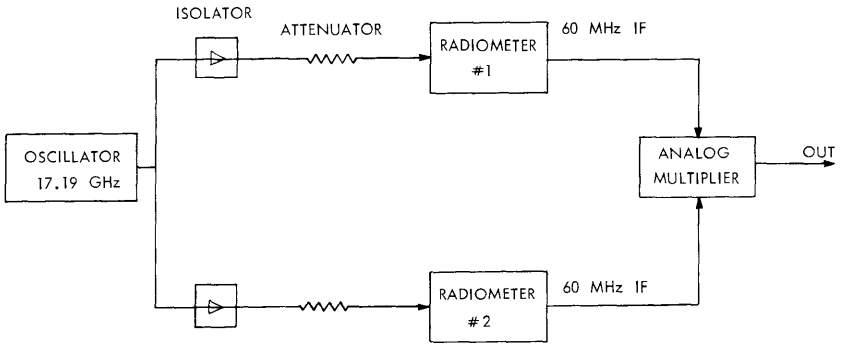

Fig. VIII-12. Experimental arrangement for phase-stability tests.

The test was performed with all of the system components (except for the antennas) used in exactly the same way as in an actual interferometric observation.

The output of the multiplier, which was monitored for approximately 2 h, is shown in Fig. VIII-13. The 180° phase shift was caused by inserting a half-wavelength delay

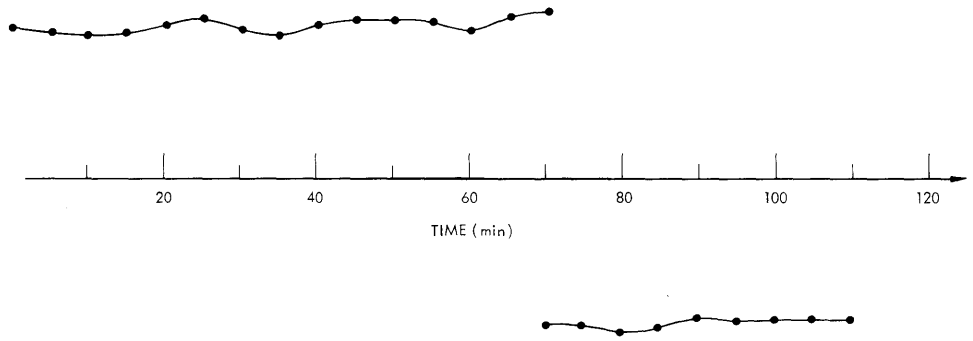

Fig. VIII-13. Multiplier output.

in one of the IF strips. Most of the random variations in the multiplier output can be attributed to the shaking of the experimental equipment by the wind. We can conclude, therefore, that the phase stability of the system over a period of 2 h is better than 10°.

Table VIII-2. Crab Nebula fringes.

Hour Angle	Fringe Components (mV)			
	In Phase		In Quadrature	
	On Source	Off	On Source	Off
1.00	93		-53	
1.25		10		-1
3.00	85		-52	
3.25		2		6

2. Observations

Consistent fringes have been obtained from the Crab Nebula. Interference has made the observation of other weaker sources difficult. In Table VIII-2 we show some of the numbers obtained from the Crab Nebula on October 30, 1969.

G. Papadopoulos, B. F. Burke

I. MICROWAVE SPECTRUM OF ATMOSPHERIC OZONE

Calculations of the microwave spectra of atmospheric oxygen and water vapor have been reported with discussions of the utilization of the spectral lines for remote sensing of the atmosphere. This report summarizes our calculations of the weaker microwave spectrum of atmospheric ozone (O_3) and briefly discusses its potential for remote sensing.

The quantum-mechanical expression for the absorption coefficient attributable to a transition between levels ℓ and m is

$$(k_\nu)_{\ell \to m} = \frac{8\pi^3}{3ck} \cdot \left(\frac{N}{T}\right) \cdot \frac{1}{Q} \cdot \mu^2 \phi^2_{\ell, m} \cdot \exp\{-E_\ell/kT\} \cdot \nu^2 \cdot f(\nu, \nu_{\ell, m}, \Delta\nu), \qquad (1)$$

where c and k are the speed of light and Boltzmann's constant, respectively, N is the number density of the absorbing molecule (O_3 in our case), T is temperature, ν is signal frequency, and μ is the dipole moment of the molecule. The transition parameters in (1) are: $\nu_{\ell, m}$ = transition frequency, E_ℓ = energy of lower state, $\phi^2_{\ell, m}$ = matrix element of the transition including level degeneracy. Our calculations are for O_3^{16} which has zero nuclear spin so that there are no nuclear spin complications of the level degeneracies. The partition function Q is given by $Q = \sum_\ell g_\ell \exp\{-E_\ell/kT\}$, where

Table VIII-3. Ozone transition parameters and computed zenith opacity for selected lines below 120 GHz.

Frequency* (GHz)	Rotational Quantum* Numbers (J, K_{-1}, K_1)		Matrix† Element ϕ^2	Lower Level‡ Energy (10^{-14} ergs)	Computed Zenith** Opacity (10^{-4} nepers)	Comments and References
	lower state	upper state				
9.201	21,2,20	20,3,17	3.01	4.06	0.6	
10.226	9,2,8	10,1,9	2.10	1.00	1.3	
11.073	3,1,3	4,0,4	1.59	0.16	1.5	
14.866	24,3,21	23,4,20	4.11	5.60	1.3	
16.163	26,4,22	27,3,25	4.39	6.86	1.2	
23.861	19,2,18	18,3,15	2.92	3.41	4.8	← A. H. Barrett et al.,[6] measurements imply $\tau \sim (2\text{-}4) \cdot 10^{-4}$
25.649	17,1,17	16,2,14	1.17	2.52	3.0	
28.960	25,3,23	24,4,20	4.18	6.00	4.6	
30.052	16,2,14	15,3,13	2.81	2.56	10.1	
30.181	15,1,15	14,2,12	1.33	2.00	6.5	
30.525	19,1,19	18,2,16	1.00	3.10	3.3	
36.023	22,3,19	23,2,22	2.99	4.78	7.4	← R. B. Mouw and Silver[7] measure $\tau \sim (20 \pm 15) \cdot 10^{-4}$
37.832	17,3,15	18,2,16	3.29	3.11	14.8	
42.83262	2,0,2	1,1,1	0.51	0.08	7.6	
43.654	13,1,13	12,2,10	1.40	1.55	13.6	
96.22884	2,0,2	2,1,1	2.48	0.05	183.2	
101.73683	4,0,4	4,1,3	4.34	0.17	345.5	← W. M. Caton et al.,[5] measurements imply $\tau \sim (320 \pm 30) \cdot 10^{-4}$
118.3643	0,0,0	1,1,1	1.00	0.00	113.1	

*From National Bureau of Standards Monograph 70, Vol. V (1968).

†Inferred from calculations by Gora.[1]

‡Calculated from slightly asymmetric prolate rotor energy expression given in text.

**For 1962 U.S. Standard Atmosphere and daytime ozone distribution of Fig. VIII-15.

g_ℓ is the ℓ-level degeneracy. For atmospheric temperatures Q may be approximated within a few per cent by

$$Q = \frac{1}{2}\left(\frac{kT}{h}\right)^{3/2}\left(\frac{\pi}{ABC}\right)^{1/2},$$

where h is Planck's constant, and A, B, C are the molecular rotational constants. The numerical values of the molecular constants are: $\mu = 0.53 \cdot 10^{-18}$ esu, A = 106.53612 GHz, B = 13.34912 GHz, C = 11.83430 GHz.[1] The transition parameters used in our calculations are given in the first five columns of Table VIII-3. The list of ozone microwave transitions in Table VIII-3 is not exhaustive, but contains some of the stronger transitions below 120 GHz. A more complete list has been given by Gora.[1] Our transition matrix elements were inferred from Gora's calculations of the line-intensity factors and, when possible, checked for consistency with the corresponding calculated matrix elements.[2] Since ozone is very nearly a prolate symmetric rotor (asymmetry parameter $\kappa = -0.97$ as compared with $\kappa = -1.00$ for a prolate rotor), E_ℓ was computed from the slightly asymmetric prolate rotor energy-level expression

$$E_\ell = E_{J,K_{-1}} = h\left[\frac{B+C}{2} \cdot J(J+1) + \frac{2A-B-C}{2} \cdot (K_{-1})^2\right].$$

The term $f(\nu, \nu_{\ell,m}, \Delta\nu)$ appearing in Eq. 1 is the line-shape factor. We used that of Van Vleck and Weisskopf.[3] In the terrestrial atmosphere the linewidth $\Delta\nu$ is due to collision and Doppler broadening.

$$\Delta\nu = \left[(\Delta\nu_{\text{collision}})^2 + (\Delta\nu_{\text{Doppler}})^2\right]^{1/2}. \tag{2}$$

The Doppler width for ozone is

$$\Delta\nu_{\text{Doppler}} = 5.17 \cdot 10^{-8}\nu T^{1/2} \qquad (T \text{ in } ^\circ\text{K}).$$

The expression that we used for the collision width is

$$\Delta\nu_{\text{collision}} = 3.96 \cdot 10^{7} P T^{-1/2} \text{ Hz}$$

for P = pressure in millibars. The collision linewidth is probably the most uncertain parameter appearing in our calculations. We assumed it to be proportional to the number of collisions which yields the $PT^{-1/2}$ dependence. The proportionality constant was inferred from indirect measurements by Walshaw,[4] who concluded that the Lorentz linewidth parameter in the 9.6-μ ozone rotational-vibrational band is 2.34 GHz for an O_3-air environment at P = 1013 mb and T = 293°K. Despite the uncertainties in assuming the

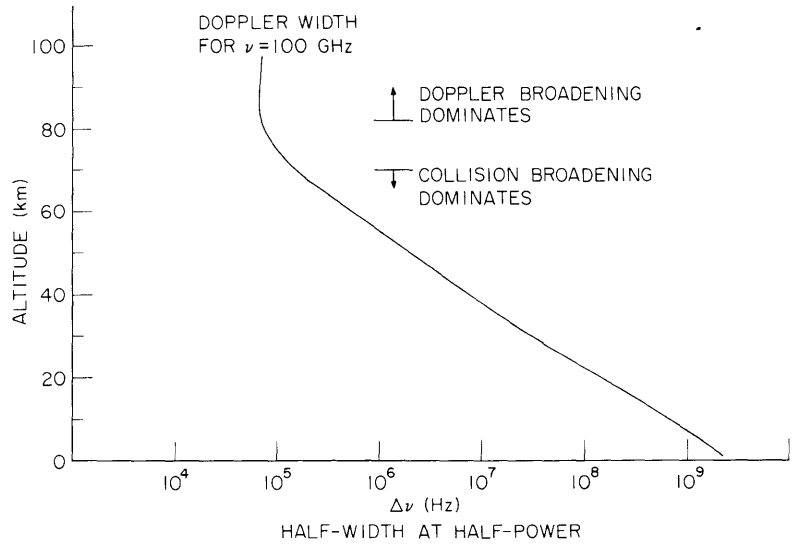

Fig. VIII-14. Computed linewidth of atmospheric O_3^{16}. (Temperature and pressure described by 1962 U. S. Standard Atmosphere.)

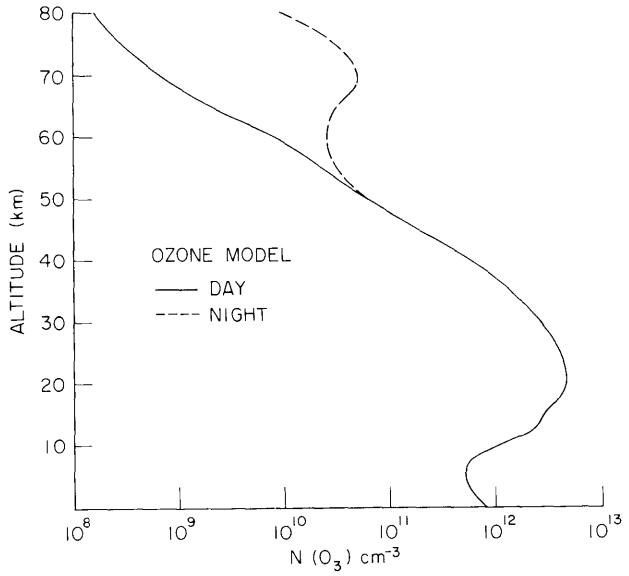

Fig. VIII-15. Ozone distribution with altitude showing diurnal variation.

expression for $\Delta\nu_{collision}$, Caton's[5] measured absorption of the 101.737 GHz ozone line gives a shape and width almost identical to that calculated by us. The calculated ozone linewidth as a function of altitude is shown in Fig. VIII-14 for ν = 100 GHz. Here, and in other calculations described below, the 1962 U.S. Standard Atmosphere was used for temperature and pressure.

The opacities at line centers were computed by numerically integrating the absorption coefficient from ground level to 80 km altitude, and are given in column 6 of Table VIII-3. A mid-latitude ozone distribution shown as the solid line of Fig. VIII-15 was used in these opacity calculations. The opacities in Table VIII-3 include absorption in the wings of lines listed in that table, but do not include absorption attributable to oxygen and water vapor.

Figure VIII-16 shows the computed brightness temperature of the 101.737 GHz line as seen looking at zenith from sea level. The line is shown both in atmospheric thermal emission and in absorption against 6000°K solar radiation. In both cases the line has been attenuated by τ = 0.3 neper, which is typical for atmospheric oxygen and water vapor at this frequency. Photochemical theory predicts a diurnal variation in ozone abundance above approximately 50 km. The theoretical nocturnal increase is shown as the dashed line of Fig. VIII-15. Such an increase in high-altitude ozone produces a relatively narrow spectral feature as has been similarly discussed for the case of water vapor. Figure VIII-17 compares our calculations of the emission spectra for the day and night ozone distributions given in Fig. VIII-15. A 101-GHz receiver with approximately 1°K sensitivity and 200-kHz frequency resolution and stability would allow convenient ground-based monitoring of the high-altitude ozone. The nocturnal ozone increase has been verified by a few isolated rocket measurements, but has not been studied in detail.

Finally, in Fig. VIII-18, we present ozone weighting functions. The weighting functions $W(\nu, h)$, which are useful for determining height resolution of remote sensing techniques, are defined by

$$T_B(\nu) = \int N(h) \cdot W(\nu, h)\, dh$$

and given by

$$W(\nu, h) = \frac{k_\nu(h)}{N(h)} \cdot T(h) \cdot \exp\left\{-\int_h^\infty k_\nu(h')\, dh'\right\},$$

where h is altitude, $T_B(\nu)$ is brightness temperature at frequency ν, and other symbols have been previously defined. The weighting functions in Fig. VIII-18 are computed for frequencies near the 37.832 GHz line and for $T_B(\nu)$ observed in emission looking at zenith from sea level. For comparison, the daytime ozone distribution is also shown

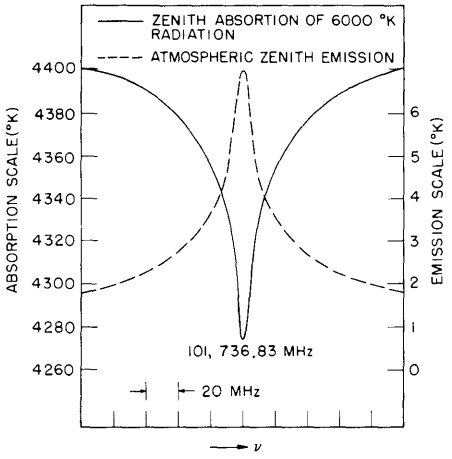

Fig. VIII-16.

Computed atmospheric absorption and emission near the 101-GHz O_3 line for the daytime ozone distribution of Fig. VIII-15. Lines have been attenuated by $\tau = 0.3$ Np because of H_2O and O_2 absorption.

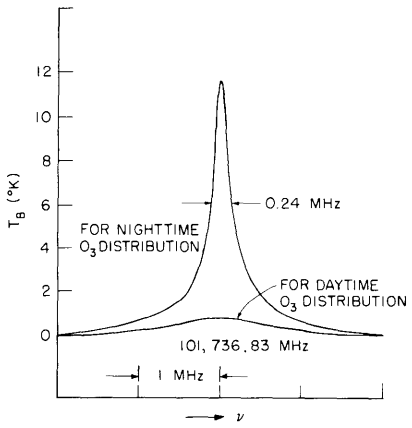

Fig. VIII-17.

Computed atmospheric zenith emission spectrum near 101.737 GHz showing nighttime enhancement caused by high-altitude ozone. An attenuation of $\tau = 0.3$ Np attributable to H_2O and O_2 has been applied. The zero level of the vertical scale has been chosen arbitrarily.

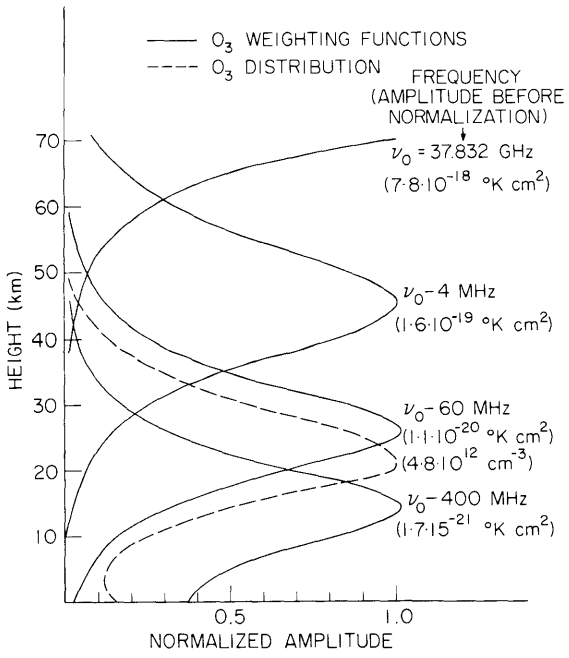

Fig. VIII-18. Ozone weighting functions computed for frequencies near the 37.832-GHz line. For comparison the ozone distribution is also shown.

in Fig. VIII-18 by the dashed line.

Calculations for the 23.861 GHz O_3 line indicate that the night-time enhancement should be detectable with the Haystack K-band radiometric system. An experiment to search for this line is now being planned.

J. W. Waters, L. D. Petro

References

1. E. K. Gora, "The Rotational Spectrum of Ozone," J. Molec. Spectros. 3, 78 (1959).
2. National Bureau of Standards Monograph 70, Vol. II, "Line Strengths of Asymmetric Rotors," U.S. Government Printing Office, Washington, D. C., 1968.
3. J. H. Van Vleck and V. F. Weisskopf, "On the Shape of Collision-Broadened Lines," Rev. Mod. Phys. 17, 227 (1945).
4. C. D. Walshaw, "Line Widths in the 9.6-μ Band of Ozone," Proc. Phys. Soc. (London) A68, 530 (1955).
5. W. M. Caton, et.al., "Radio Measurement of the Atmospheric Ozone Transition at 101.7 GHz," Astrophys. J. 151, L153 (1968).
6. A. H. Barrett, R. W. Neal, D. H. Staelin, and R. M. Weigand, "Radiometric Detection of Atmospheric Ozone," Quarterly Progress Report No. 86, Research Laboratory of Electronics, M.I.T., July 15, 1967, p. 26.
7. R. B. Mouw and S. Silver, "Solar Radiation and Atmospheric Absorption for the Ozone Line at 8.3 mm," Space Sciences Laboratory, Series No. 1, Issue No. 1, University of California at Berkeley, June 30, 1960.

J. SEARCH FOR STRATOSPHERIC H_2O ABSORPTION WITH THE HAYSTACK ANTENNA

During the past several months, the Haystack antenna and K-band spectrometer system have been used in an attempt to measure the relatively narrow absorption feature at 22.235 GHz expected from water vapor in the stratosphere of the Earth. Thus far, no spectral feature has been observed which can definitely be attributed to atmospheric absorption. Our limit on the line strength, for the 4-MHz bandwidth of the spectrometer, is given in Fig. VIII-19 as a function of elevation angle for several days of observation. The observed antenna temperature was converted to brightness temperature by using 10,000°K for the solar brightness temperature. The sensitivity of these measurements is limited by the nonflat frequency baseline of the spectrometer when used for observing the sun. This instrumental baseline varies with elevation and with signal strength, and is not reduced by averaging data.

Also shown in Fig. VIII-19 is the signal strength expected for various amounts of water vapor extending to an altitude of 60 km. From these measurements we infer

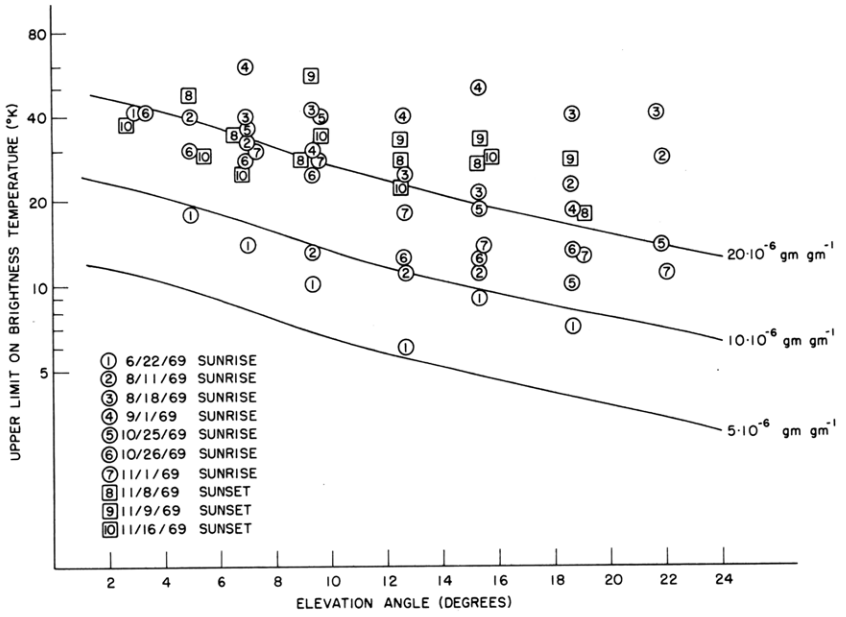

Fig. VIII-19. Upper limits on 4-MHz wide absorption feature at 22, 235 MHz in the solar spectrum. Solid lines show expected line strength for indicated stratospheric H_2O mixing ratio extending to 60 km.

an upper limit on stratospheric water vapor which is approximately 10 times that inferred from our measurements made at the National Radio Astronomy Observatory last summer.[1]

J. W. Waters, M. L. Meeks, D. H. Staelin

(Dr. M. L. Meeks is with Lincoln Laboratory, M. I. T.)

References

1. J. W. Waters and D. H. Staelin, "Search for the 1.35-cm Stratospheric H_2O Line," Quarterly Progress Report No. 95, Research Laboratory of Electronics, M. I. T., October 15, 1969, pp. 6-7.

K. DISPERSION NEAR 22.235 GHz CAUSED BY STRATOSPHERIC WATER VAPOR

Using Liebe's[1] expression for the refractive index of water vapor near the 22.235 GHz (1.35 cm) resonance, we computed the integrated dispersion expected from stratospheric water vapor, and it is shown in Fig. VIII-20a. A stratospheric mixing ratio of $2 \cdot 10^{-6}$ gm H_2O per gm air, which is the approximate upper limit set by our observations of atmospheric thermal emission,[2] was used in the calculations. A typical

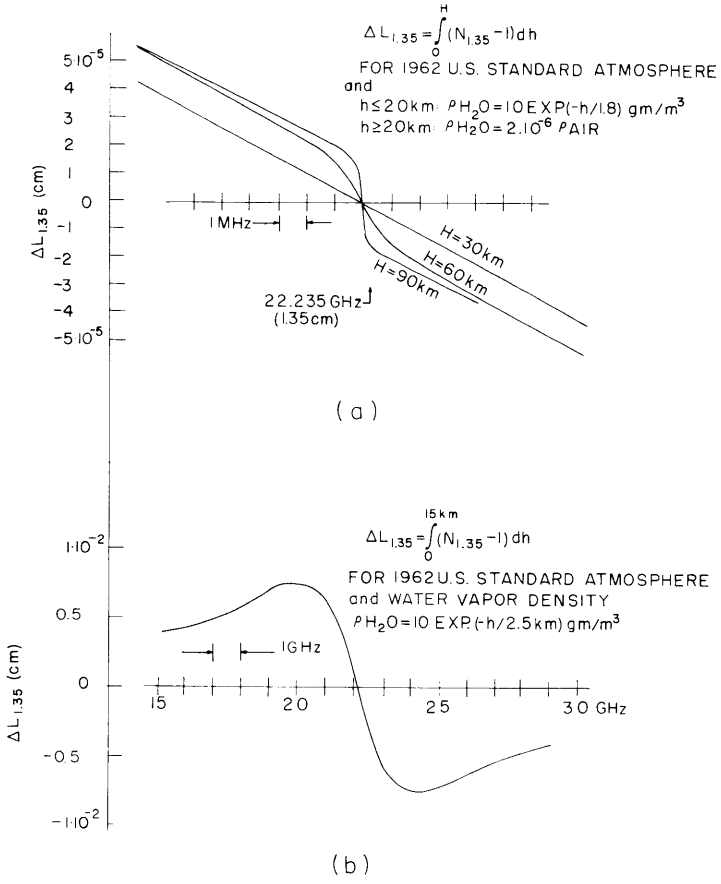

Fig. VIII-20. (a) Stratospheric H_2O contribution to dispersion for mixing ratio of $2 \cdot 10^{-6}$ gm gm^{-1}.
(b) Tropospheric zenith dispersion.

distribution of water vapor in the troposphere was used. Three curves are shown for water vapor extending to altitudes of 30, 60, and 90 km, respectively. These curves indicate that a dispersion experiment to measure stratospheric water vapor must be able to measure an effective path change of 10^{-5} cm over a 1-MHz frequency range, and hence is not feasible. Calculations of tropospheric dispersion are shown in Fig. VIII-20b, and agree with the calculations of Liebe.[1]

J. W. Waters

References

1. H. J. Liebe, "Calculated Tropospheric Dispersion and Absorption Due to the 22-GHz Water Vapor Line," IEEE Trans., Vol. AP-17, pp. 621-627 (September 1969).
2. J. W. Waters and D. H. Staelin, "Search for the 1.35-cm Stratospheric H_2O Line," Quarterly Progress Report No. 95, Research Laboratory of Electronics, M.I.T., October 15, 1969, pp. 6-8.